DOI: 10.1002/ejic.200701008

Effects of Precipitation, Sol–Gel Synthesis Conditions, and Drying Methods on the Properties of Nano-TiO_2 for Photocatalysis Applications

Chabaiporn Junin,[a] Chanchana Thanachayanont,[a] Chanipat Euvananont,[a] Kroekchai Inpor,[b] and Pimpa Limthongkul*[a]

Keywords: Titanium / Sol–gel / Precipitation / Freeze drying / Photocatalysis

A comparative study of TiO_2 powders prepared by precipitation and sol–gel methods was conducted. Titanium tetrachloride and titanium tetraisopropoxide were used as the starting materials for the precipitation and sol–gel processes, respectively. The effects of the two different drying methods, freeze drying and normal drying at 100 °C, of the precipitates on the properties of the prepared TiO_2 powders were also investigated. The effects of the synthesis methods on phase, surface area, crystallite size, and photodegradation of methylene blue were studied by XRD, SEM, TEM, BET, and UV/Vis techniques. It was found that the major phase of the synthesized TiO_2 was anatase, but small amounts of the brookite phase (<10 %) were found in some samples. The synthesized anatase TiO_2 with no pretreatment was found to be stable up to 600 °C for the samples prepared by the precipitation method, whereas a small amount of rutile was detected for the sample prepared by the sol–gel method when heated to 600 °C. Effects of the different processing methods on phase, particle size, surface area, and photocatalytic activity were not highly pronounced. However, the calcination temperature was found to have a strong influences on the properties. As the calcination temperature increased, the size of the crystallite and the percent degradation of methylene blue were found to increase, whereas the surface area was found to decrease. These results indicate the degree of crystallinity has a greater effect on the photocatalytic activity than the surface area for nano-TiO_2 synthesized by these methods.

Introduction

Titanium dioxide, TiO_2, is useful in various applications ranging from pigments for paint[1,2] to dielectric, photovoltaic,[3] and gas sensor[4,5] applications. Recently, TiO_2 has gained much attention as the material of choice for environmental-related applications such as air purification,[6] water treatment,[7,8] and self cleaning[9] due to its photocatalytic properties, along with its stability and low cost.

The photocatalytic activity of TiO_2 depends on the availability of active sites, and, thus, depends on surface area, surface defect, surface acidity, and degree of crystallinity.[6,10] Besides the mentioned properties, the crystalline structure of TiO_2 was also found to be important. TiO_2 exists in three polymorphic forms: rutile, anatase, and brookite, among which rutile is the thermodynamically stable phase, whereas the latter two phases are metastable.[11] Previous work on TiO_2 photocatalysts suggested that TiO_2 with the anatase structure exhibits substantially higher photocatalytic activity than TiO_2 in the amorphous or rutile phases as a result of its slightly higher Fermi level, lower capacity to adsorb oxygen, and higher degree of hydroxylation.[12,13] It was also reported that highly crystalline anatase had a higher adsorptive affinity for organic compounds and exhibited a lower recombination rate than rutile.[14,15] Some studies reported that a mixture of anatase and some other phases such as brookite or rutile as the minor phase offered a superior photocatalytic activity than a single-phase TiO_2.[16,17] In mixed phases, a study by Hurum et al.[18] showed that rutile, which has a smaller bandgap than anatase (3.0 eV for rutile and 3.2 eV for anatase), could act as an antenna that could produce charges under visible light, and the generated charges could be stabilized by electron transfer to the anatase phase. Several reports suggest that the optimum photoactivity is influenced by many different important factors, such as surface area and degree of crystallinity, as mentioned above.

Because the properties of TiO_2 are highly affected by the synthesis conditions and heat treatments, many processing routes such as sol–gel,[19] hydrothermal,[20] and hydrolysis of inorganic salts[21] have been proposed with the aim to obtain desirable morphologies and properties. Efforts have also been put forth to stabilize anatase above 550 °C to obtain highly crystallized anatase; however, those efforts including the use of the sulfate group during the synthesis.[20,22]

[a] National Metal and Materials Technology Center, 114 Thailand Science Park, Paholyothin Rd., Klong 1, Klong Luang, Pathumthani 12120, Thailand
Fax: +66-2-564-6447
E-mail: pimpal@mtec.or.th
[b] Institute of Solar Energy Technology Development, 111 Thailand Science Park, Paholyothin Rd., Klong 1, Klong Luang, Pathumthani 12120, Thailand

EurJIC European Journal of Inorganic Chemistry

In this work, a more simple process with the aim to stabilize nanocrystalline anatase TiO_2 by the precipitation method along with a more complex sol–gel route are investigated. The effects of the different synthesis routes on the crystal structure, morphology, surface area, and photocatalytic efficiency towards degradation of methylene blue are studied. Freeze drying has been known as one of the drying methods that could yield mixed oxides with large surface areas.[23] In this study, the effects of two different drying methods, drying at 100 °C and freeze drying, on the properties TiO_2 are also investigated.

Results and Discussion

Phase Formation Analysis

Figure 1 top, middle, and bottom show XRD patterns of the calcined TiO_2 powders prepared by the sol–gel method, the precipitation method dried at 100 °C, and the precipitation method freeze dried, respectively. It was found that anatase TiO_2 was the major phase under all synthesis conditions and at all calcination temperatures. For the sol–gel-synthesized powder, a small amount of the brookite phase between 6–7 wt.-% was found to coexist with the anatase phase at temperatures between 400 and 500 °C, as observed by the broad small peak at 2θ = 30.8°. At 600 °C, small peaks corresponding to rutile TiO_2 were observed and decreasing relative intensities of anatase and brookite were found. The weight percent of the newly formed rutile phase at 600 °C was found to be 10 wt.-%.

For the powder prepared by the precipitation method, the anatase phase was found to be stable even when heated up to 600 °C for 2 h without any additional pretreatment. However, there was a slight difference in the phases found between the samples dried at 100 °C and the freeze dried samples. Whereas it was found that anatase TiO_2 existed as a single phase at all calcination temperatures for the freeze-dried samples, and for the samples dried and calcined at 400 and 600 °C, a small amount of the brookite phase was also detected for the sample dried at 100 °C and calcined at 500 °C. The appearance and disappearance of brookite at different calcination temperatures might be explained by a small activation energy (only 11.9 kJ mol^{-1}) for the transformation between the two phases.[24]

It is to be noted that the transformation of anatase into rutile, which was observed at 600 °C for the sol–gel-synthesized sample but not for the precipitated samples, might arise from the different synthesis method yielding samples with different degrees of crystallinity at low temperature. Figure 2 shows the XRD patterns of the dried but not calcined samples synthesized by the sol–gel (top) and precipitation (bottom) methods. Only short-range ordering was found for the precipitated sample, whereas peaks corresponding to the anatase and brookite phases could clearly be seen. This early stage of crystallization might lead to a faster increase in crystallite size in the sol–gel-derived samples relative to the precipitated samples. As when the size is above the critical size (>35 nm) for the anatase or brookite

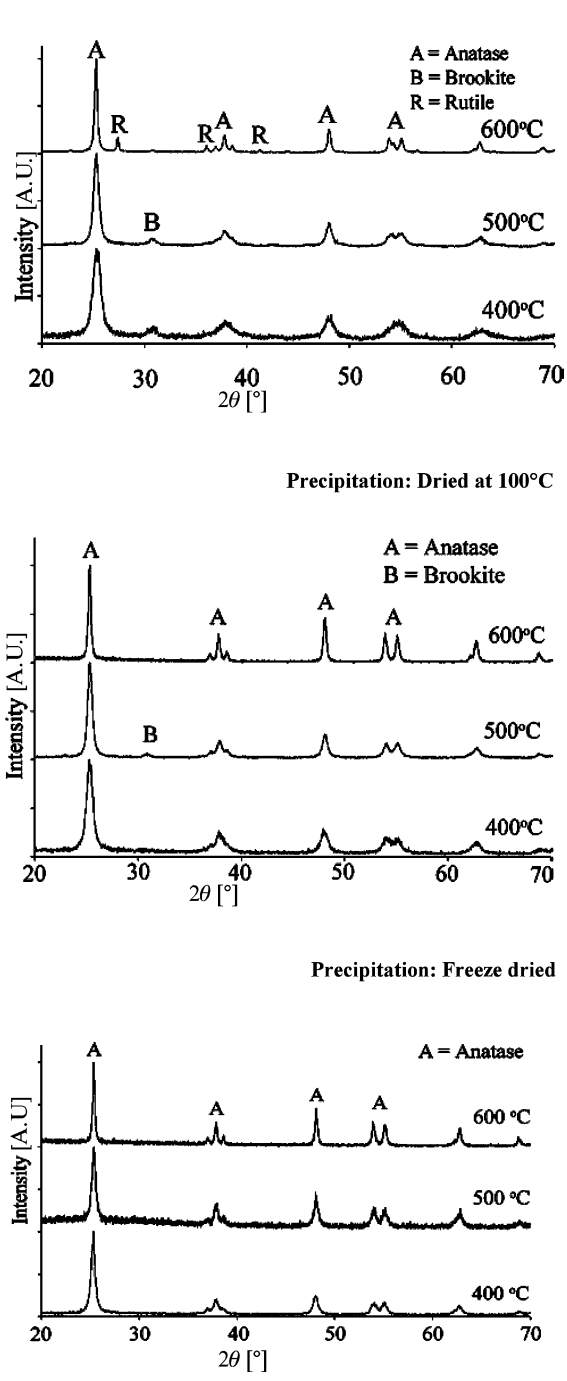

Figure 1. XRD pattern of TiO_2 powders prepared by the sol–gel method followed by drying at 100 °C and the precipitation method followed by freeze drying at –45 °C at different calcination temperatures.

phases to be stable, the more thermodynamically stable rutile phase is expected to form.[24] It was also reported that the existence of brookite enhances the anatase to rutile phase transformation due to high interfacial energy between the anatase and brookite phases.[25,26] In the sol–gel-synthesized samples, a larger amount of the brookite phase was found relative to that found in the samples produced by the precipitation method.

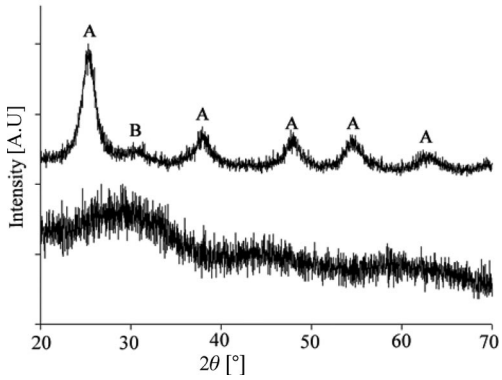

Figure 2. XRD patterns of the dried, but not calcined powders prepared by precipitation (bottom) and sol–gel (top) methods.

Morphology and Crystallite Size Analysis

Images of the morphologies of the TiO_2 powders under SEM are presented in Figure 3. It can be seen that all the samples exist in a highly agglomerated form despite the synthesis method used or the drying process employed; all samples were obtained as very fine powders with particle sizes in the nanometer range.

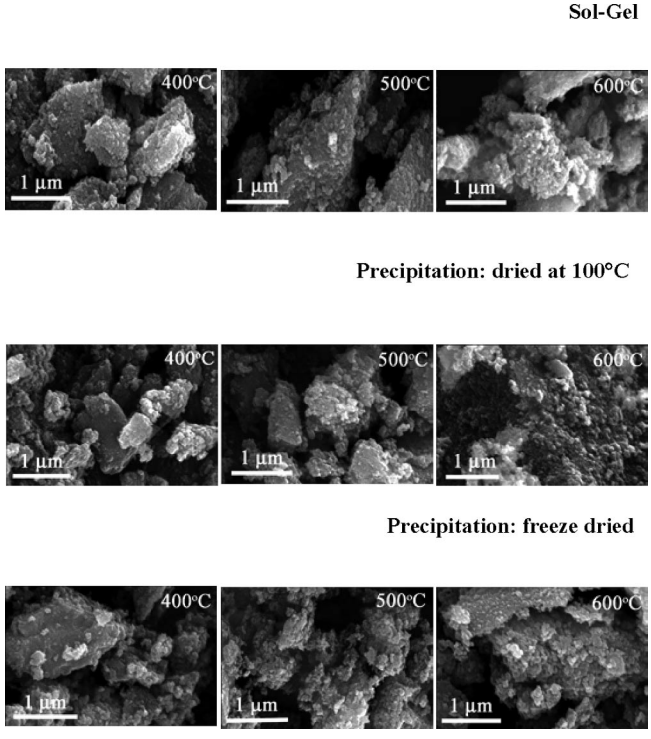

Figure 3. SEM micrographs of the synthesized powder calcined at 400, 500, and 600 °C for 2 h.

Further investigation into the size and morphology of the particle was investigated by TEM. From Figure 4, it can be seen that for all samples, independent of the methods and drying processes used, individual TiO_2 particles calcined at 400 °C are less than 15 nm in size, whereas the ones calcined at 500 °C are slightly larger in size (15–20 nm). For the powder subjected to heat treatment at 600 °C, large particles greater than 20 nm in size were obtained. The average crystallite size obtained from both drying processes and both synthesis methods was carried out from a fringe pattern. The average crystallite sizes calculated from the TEM micrographs and from the broadening of the XRD peaks are presented in Table 1. The values from both methods are close to each other, although the values presented from the XRD results are only from the (101) peak of anatase TiO_2. As the calcination temperature increased, the size of the crystallite also increased, as expected. For the sol–gel powder calcined at 600 °C where TiO_2 in the rutile form was also found, the calculated particle size of the rutile phase was found to be slightly larger, approximately 38 nm. The results from this work are consistent with those of Zhang, et al.,[24] in which the critical size for the transformation into rutile is >35 nm.

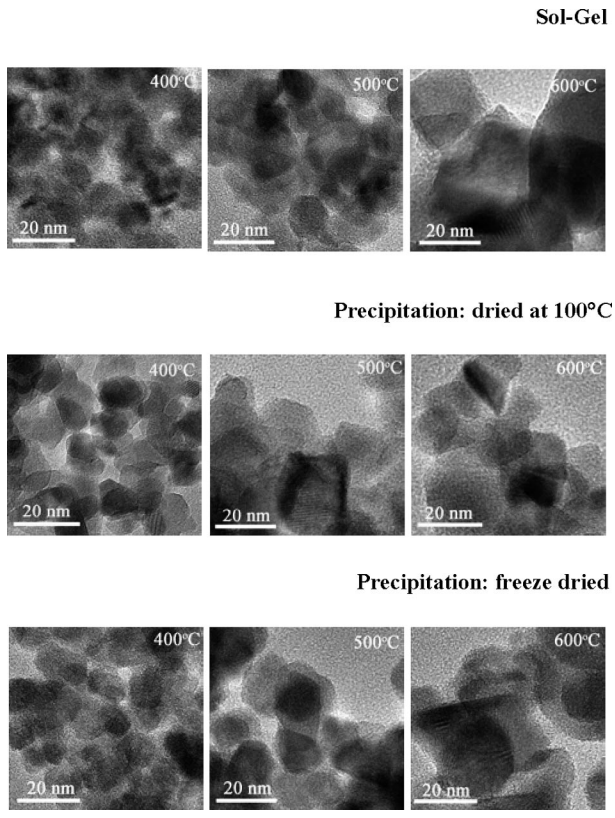

Figure 4. TEM micrographs of the synthesized powder calcined at 400, 500, and 600 °C for 2 h.

The surface area of the synthesized TiO_2 was found to be in agreement with the results from the XRD and TEM analysis (Table 2). As the calcination temperature increased, the surface area was found to decrease. The surface areas of the powders synthesized by the sol–gel method and the precipitated freeze-dried powder are in the same range: 90–100 $m^2 g^{-1}$ for 400 °C, 70 $m^2 g^{-1}$ for 500 °C, and 30 $m^2 g^{-1}$ for 600 °C calcination temperatures. The precipitated powders dried at 100 °C have slightly smaller surface areas of 72, 57, and 23 $m^2 g^{-1}$ when calcined 400, 500, and 600 °C, respectively.

Table 1. Crystallite size of TiO_2 synthesized by the precipitation method, followed by different drying processes, and by the sol–gel method.

Calcination	Crystallite size from XRD[a] [nm]			Crystallite size from TEM [nm]		
Temperature [°C]	Precipitation / 100 °C	Precipitation / Freeze dried	Sol–gel	Precipitation / 100 °C	Precipitation / Freeze dried	Sol–gel
400	13	13	11	11	12	11
500	18	20	16	18	19	19
600	29	35	29	32	26	31
P25		21(anatase) 37 (rutile)			27	

[a] Calculated from the (101) peak of the anatase phase only.

Table 2. Surface area and photoactivity of TiO_2 synthesized by the precipitation method, followed by different drying processes, and by the sol–gel method.

Calcination	Surface area [$m^2 g^{-1}$]			Degradation of methylene blue [%]		
Temperature [°C]	Precipitation / 100 °C	Precipitation / Freeze dried	Sol–gel	Precipitation / 100 °C	Precipitation / Freeze dried	Sol–gel
400	72	98	94	21	15	15
500	57	75	72	34	19	32
600	23	36	30	39	45	44
P25		59			38	

Photocatalytic Activity Analysis

The effects of the preparation method, calcination temperature, particle size, and surface area of the prepared samples on photocatalytic activity were investigated. The results are shown in Table 2. Photocatalytic performances of the powders were tested against commercial TiO_2 (Degussa, P25) for comparison. By comparing the photocatalytic activities of the samples prepared by the precipitation and sol–gel methods, although the different methods yield a slightly different particle size and surface area, it was found that no significant difference in photocatalytic activity between the different synthesis methods could be observed. Calcination temperature, however, seemed to have a strong effect on the degradation of methylene blue. As the calcination temperature increased from 400 to 600 °C, not much phase change was observed. However, a significant increase in particle size and a significant decrease in surface area were found. Photocatalytic activity was also found to increase with an increase in calcination temperature.

This is in contrast to what was observed in some earlier reports where higher surface areas resulted in a larger area for reactions and, thus, higher activity or increased particle sizes resulted. Therefore, by lowering the surface area, the number of hydroxy groups on the surface of the catalyst is reduced, which results in lower catalytic activity.[27–29]

The results, however, could be explained by looking at the effects of different steps that occur during the photocatalytic reactions, which can be divided into two main parts.[30] The first part involves what occurs in the TiO_2 particles, and this includes photon absorption, electron–hole generation, and electron–hole trapping. The second part involves foreign species and reactions at the surface; this includes, surface absorption and radical formation, reactions of the surface species with pollutants, and removal of reacted species. The first part is mainly affected by parameters of the materials such as phase, degree of crystallinity, bulk, and surface defects. The second part, however, is likely to be mainly affected by parameters such as surface acidity, surface area, concentration of the pollutant, and so on. Both parts will always be in competition, as small, high-surface-area particles are usually associated with less-ordered structures and a high concentration of defects, which favor the recombination of electrons and holes, which in turn leads to poor photoactivity;[6] a surface area that is too low will not provide enough sites for absorption. In our case, the observation of increasing photocatalytic activity with increasing calcination temperature, decreasing surface area, and increasing crystallite size combined with the lack of differences in the phases of the different powders indicates that the first step in the photocatalysis reaction is the limiting step. The efficiency of the synthesized powder in the degradation of methylene blue was found to be slightly higher than that of the commercial P25 when calcined at 600 °C.

Conclusions

An attempt to synthesize stable anatase TiO_2 with no pretreatment was successful in this study. Anatase was found to form at an early stage of synthesis for the sol–gel method and was found to be the major phase in all samples synthesized. Anatase was found to be stable up to 600 °C, and small amounts of brookite existed as the minor phase in some of the samples. Phase transformation of anatase into rutile was only observed in the sample synthesized by the sol–gel method when calcined at 600 °C. As the calcination temperature increases, crystallite size increased and surface area decreased as expected. Different synthesis methods, precipitation and sol–gel, and drying processes,

normal drying at 100 °C and freeze drying at –45 °C, on the properties of TiO_2 powders were not found to have a strong influence on crystallite size, surface area, and photocatalytic activity. Photocatalytic activity, however, was highly dependent on the calcination temperature, which is directly related to the degree of crystallinity.

Experimental Section

TiO_2 powders were prepared by the precipitation and sol–gel methods. For the samples prepared by precipitation method, titanium tetrachloride (6.8 mL, 99% $TiCl_4$, Merck) was hydrolyzed by slowly adding the chloride solution onto ice cubes (30 mL of DI-water) and stirring vigorously until a clear solution was obtained. Ammonium hydroxide solution (25 mL, 30% NH_4OH, Merck) was then slowly added to the mixture with constant stirring until a white precipitate formed. The precipitate was then washed with deionized water several times until pH 8 was reached to eliminate chloride and ammonium ions. The drying step was done in two different ways: freeze drying (–45 °C) for 24 h and drying in air at 100 °C for 72 h. The white powders were calcined at 400, 500, and 600 °C for 2 h to obtain TiO_2 powder. For the sol–gel method, titanium(IV) isopropoxide precursor (45.3 g, TTIP, Fluka) was diluted in 2-propanol (12.5 mL, IPA, Fluka), and 0.1 M HNO_3 (75 mL, HNO_3 65%, Lab-Scan) was added to the mixture, which resulted in immediate precipitation. The precipitate was peptized at 60 °C for 8 h in a reflux system. The solution was then left to stir at room temperature for 12 h, followed by the evaporation of 2-propanol and water at 55 °C for one week to obtain xerogel. Calcination of the precipitated powder and the xerogel was carried out at 400, 500, and 600 °C for 2 h in air to obtain TiO_2 powder.

X-ray diffraction analysis (XRD, Cu-K_α, JEOL JDX-3530) was performed to study the crystal structures, crystallite sizes, and phase formations of the prepared samples. The crystallite size of the samples was determined by the Sherrer equation:

$$L = \frac{\lambda k}{B \cos\theta}$$

where θ is the Bragg's angle, B is the broadening of the peak at half maximum intensity, L is the crystal size, and k is the constant ≈ 0.94. The amount of each phase was quantified by the equations proposed by Zhang, et al.:[24]

$$W_R = \frac{I_R}{I_R + k_A I_A + k_B I_B}$$

$$W_A = \frac{k_A I_A}{I_R + k_A I_A + k_B I_B}$$

$$W_B = \frac{k_B I_B}{I_R + k_A I_A + k_B I_B}$$

where W_R, W_A, and W_B represent the weight fractions of the rutile, anatase, and brookite phases, respectively; I_R is the integrated intensity of the (110) rutile peak; I_A is the integrated peak intensity of the (101) anatase TiO_2; and I_B is the integrated intensity of the (121) brookite peak; k_A is equal to 0.886 and k_B is equal to 2.721.

The morphology and crystallite size of the TiO_2 powders were investigated by scanning electron microscopy (SEM, JEOL JSM-6310F) and transmission electron microscopy techniques (TEM, JEOL JEM-2010). Specific surface areas of the samples were determined by the Branauer–Emett–Teller (BET) method (Autosorb, Quantachrome).

The photocatalytic activity of TiO_2 was evaluated by investigating degradation of methylene blue (MB, Riedel-deHaën), which was used to represent a pollutant. For the photodegradation investigation, TiO_2 powder (5 mg) was added to an aqueous solution of methylene blue (6.25×10^{-5} M, 10 mL). The sample was stirred continuously while it was irradiated with UV light (long-wavelength mode; 365 nm) for 2 h. After irradiation, the mixture was centrifuged at 8000 rpm for 5 min to remove TiO_2 particles, and a clear solution was obtained. Degradation of the pollutant was then determined by measuring the absorbance of methylene blue of each decanted solution by using a UV/Vis spectrophotometer (JASCO V-530) at λ_{max} = 661 nm.

Acknowledgments

We would like to thank the National Metal and Material Technology Center for financial support (MTEC Grant No. MT-B-48-CER-07-187-I).

[1] F. Tiarks, T. Frechen, S. Kirsch, J. Leuninger, M. Melan, A. Pfau, F. Richter, B. Schuler, C.-L. Zhao, *Prog. Org. Coat.* **2003**, *48*, 140–152.
[2] S. Croll, *Prog. Org. Coat.* **2002**, *44*, 131–146.
[3] T. A. Heimer, C. A. Bignozzi, G. J. Meyer′pt, *J. Phys. Chem.* **1993**, *97*, 11987–11994.
[4] C. Garzella, E. Comini, E. Tempesti, C. Frigeri, G. Sberveglieri, *Sens. Actuators B* **2000**, *68*, 189–196.
[5] A. M. Ruiz, G. Sakai, A. Cornet, K. Shimanoe, J. R. Morante, N. Yamazoe, *Sens. Actuators B* **2003**, *93*, 509–518.
[6] O. Carp, C. L. Huisman, A. Rell, *Prog. Solid State Chem.* **2004**, *32*, 33–177.
[7] A. Fujishima, K. Honda, *Nature* **1972**, *238*, 37–38.
[8] S. N. Frank, A. J. Bard, *J. Am. Chem. Soc.* **1977**, *99*, 303–304.
[9] R. Blossey, *Nat. Mater.* **2003**, *2*, 301–306.
[10] A. Sclafani, J. M. Hermann, *J. Phys. Chem.* **1996**, *100*, 13655–13661.
[11] Y. M. Wang, S. W. Liu, M. K. Lü, S. F. Wang, F. Gu, X. Z. Gai, X. P. Cui, J. Pan, *J. Mol. Catal. A* **2004**, *215*, 137–142.
[12] A. Di Paola, G. Marci, L. Palmisano, M. Schiavello, K. Uosaki, S. Ikeda, B. Ohtani, *J. Phys. Chem. B* **2002**, *106*, 637–645.
[13] K. Tanaka, M. F. V. Capule, T. Hisanag, *Chem. Phys. Lett.* **1991**, *187*, 73–76.
[14] U. Stafford, K. A. Gray, P. V. Kamat, A. Varma, *Chem. Phys. Lett.* **1993**, *205*, 55–61.
[15] G. Riedel, J. R. Bolton, *J. Phys. Chem.* **1995**, *99*, 4215–4224.
[16] J. Yu, J. C. Yu, M. K.-P. Leung, W. Ho, B. Cheng, X. Zhao, J. Zhao, *J. Catal.* **2003**, *217*, 69–78.
[17] S. Ito, S. Inoue, H. Kawada, M. Hara, M. Iwasaki, H. Tada, *J. Colloid Interface Sci.* **1999**, *216*, 59–64.
[18] D. C. Hurum, A. G. Agrios, K. A. Gray, *J. Phys. Chem. B* **2003**, *107*, 4545–4549.
[19] G. Colon, M. C. Hidalgo, J. A. Navio, *Catal. Today* **2002**, *76*, 91–101.
[20] M. Inagaki, Y. Nakazawa, M. Hirano, Y. Kobayashi, M. Toyoda, *Int. J. Inorg. Mater.* **2001**, *3*, 809–811.
[21] Y. Zhang, G. Xiong, N. Yao, W. Yong, X. Fu, *Catal. Today* **2001**, *68*, 89–95.
[22] Y. V. Kolen'ko, A. A. Burukhin, B. R. Churagulov, N. N. Oleynikov, *Mater. Lett.* **2003**, *57*, 1124.
[23] A. Vargas, J. A. Montoya, C. Maldonado, I. Hernández-Pérez, D. R. Acosta, J. Morales, *Microporous Mesoporous Mater.* **2004**, *74*, 1–10.
[24] H. Zhang, J. F. Banfield, *J. Phys. Chem. B* **2000**, *104*, 3481–3487.
[25] H. Zhang, J. F. Banfield, *J. Mater. Chem.* **1998**, *8*, 2073–2076.

[26] J. F. Banfield, B. L. Bischoff, M. A. Anderson, *Chem. Geol.* **1993**, *110*, 211–231.
[27] W. Y. Teoh, L. Madler, D. Beydoun, S. E. Pratsinis, R. Amal, *Chem. Eng. Sci.* **2005**, *60*, 5852–5861.
[28] C. Randorn, S. Wongnawa, P. Boonsin, *Science Asia* **2004**, *30*, 149–156.
[29] S. S. Watson, D. Beydoun, J. A. Scott, R. Amal, *Chem. Eng. J.* **2003**, *95*, 213–220.
[30] S. Boujday, F. Wunsch, P. Portes, J.-F. Bocquet, C. Colbeau-Justin, *Sol. Energy Mater. Sol. Cells* **2004**, *83*, 421–433.

Received: September 18, 2007
Published Online: January 15, 2008

